

Finite Element of Composite Reinforced Concrete Slender Columns Subjected to Eccentric Loads

Zaynab S. Mohammed^{1*}, Bassman R. Muhammad¹ and Ali S. Reshaq¹

¹Civil Engineering Departement-University of Technology , Baghdad, Iraq.

Abstract. The relationship between reinforced concrete column tests and finite element behavior is crucial for understanding and optimizing the structural performance of these elements. Concrete columns are integral components in buildings and infrastructure, and testing them under various conditions provides valuable data on their strength, stiffness, and failure mechanisms. Finite element analysis, on the other hand, is a powerful numerical method used to simulate the complex behavior of structures under different loads. By correlating experimental results from concrete column tests with finite element models, engineers can validate and refine their simulations, ensuring that the computational models accurately represent the physical reality. This iterative process of testing and analysis allows for the development of more reliable and efficient design methodologies, leading to improved structural performance and safety in construction projects. The synergy between experimental testing and finite element behavior not only enhances our understanding of structural dynamics but also contributes to the advancement of innovative and resilient construction practices. The results shows a good coincidence between the experimental and theoretical results.

1 Introduction

The steel column enclosed in concrete is made up of a steel rolling geometric section that is either fully or partially encased in reinforced concrete at the center. A centrally encased steel section enhances the concrete column's axial load carrying capacity and eliminates local buckling[5].

In addition to improving fire resistance, having a smaller cross-section, and being more cost-effective for high-rise buildings, the centrally encased steel-concrete column also increases ductility, stiffness, energy absorption capacity, confined concrete zone, and load-carrying capacity. It also saves time as well as funds on construction materials [14].

Several experimental studies involving the application of various loads on composite columns have been conducted.

Many researchers have focused on composite enclosed columns with I-shaped steel structural sections, despite the fact that the behaviors of centrally enclosed steel-concrete composite columns have been thoroughly examined.

Composite constructions typically use alternative shapes of steel sections, such as U, L, T, or cross shapes. In recent years, scientists are using various configurations of structural steel sections to examine a number of factors influencing the behavior of composite columns. These several factors could include steel section ratios, various steel section types and shapes, repercussions of concrete confinement, axial-load ratio, and material strength[14].

The finite element method has developed into a potent and practical tool for the analysis of numerous engineering issues in recent years. The number of experiments can be significantly decreased because of to the thorough finite element model. Nonetheless, a thorough examination of any structural system must include an experimental phase. For finite element models to produce failure outcomes that can be relied on, the component parts must be accurately represented, suitable elements must be used, and appropriate solution techniques must be applied [9].

*Corresponding author: zaynabsabah20@gmail.com

In this research, the Abacus program was used to understand, study and evaluate the response of slender concrete columns installed on the basis of the damaged concrete plasticity model. To address the lapses and shortcomings in numerical studies for this type of columns, a numerical model based on the finite element method was developed. This study displays the analytical model specifics to track the performance of reinforced concrete encased steel slender columns and compare it with reinforced concrete slender columns.

2 Methodology

In the experimental part of this research, twelve reinforced RC columns with six of them steel embedded channel section were constructed. All columns have a 150×200 mm cross-sectional area and a length of 1600, 1800 and 2000 mm with a 300 mm corbel at each end as shown in Figure (1). The clear height of the columns is 1000, 1200 and 1400 mm respectively and $6\text{Ø}10$ mm used as longitudinal reinforcement, and $\text{Ø}6$ mm spaced of 75 mm is used as tie reinforcement. Six C3 \times 5 channel steel section is inserted longitudinally inside each column. Three-dimensional models of each specimen were created using the ABAQUS/CAE interface. Table (1) represents the full details of columns properties.

In order to account for the effects of various geometric characteristics that can have a substantial impact on the behavior of Finite Element columns, the columns used in this study were constructed and examined during the parametric analysis.

The current study's primary goal was to examine the load carrying capacity, ductility and deflection of the slender columns with encased composite slender columns due to the eccentric load applied. Moreover, Comparing the efficacy of nonlinear analysis of FE results with experimental data is the aim of model validity.

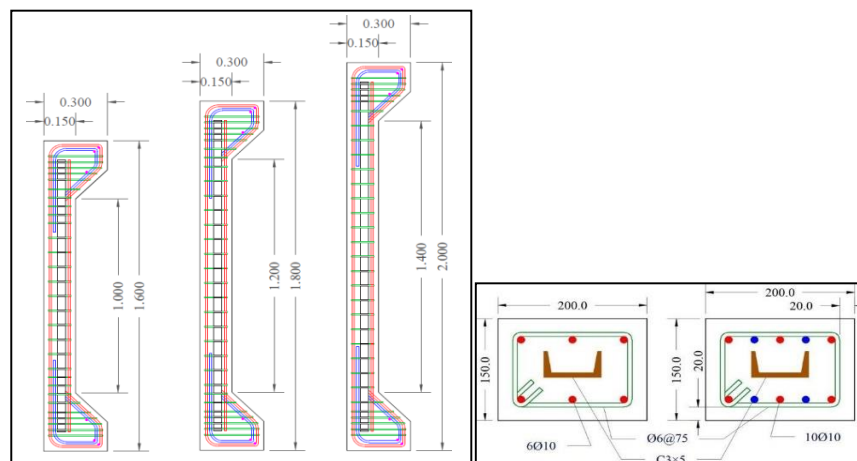


Fig. 1. Dimensions of columns, both longitudinally and cross-sectionally.

Table 1. Column Specimens Properties

Group No.	Specimen No.	Column Designation*	l_u (m)	Slenderness Ratio l_u / r	e/h	Steel Section
A	1	C0E45L1.0	1.0	22.22	0.3	0
	2	C0E45L1.2	1.2	26.67		
	3	C0E45L1.4	1.4	31.11		
	4	C0E90L1.0	1.0	22.22	0.6	
	5	C0E90L1.2	1.2	26.67		
	6	C0E90L1.4	1.4	31.11		
B	7	C1E45L1.0	1.0	22.22	0.3	1
	8	C1E45L1.2	1.2	26.67		
	9	C1E45L1.4	1.4	31.11		
	10	C1E90L1.0	1.0	22.22	0.6	
	11	C1E90L1.2	1.2	26.67		
	12	C1E90L1.4	1.4	31.11		

3 Finite Element Modeling for the Tested Specimens

An overview of the specifics of the column modeling using the finite element approach is provided in this paragraph. For this goal, popular software [19] was utilized.

3.1 Material Modeling

The model defines the material parameters for steel reinforcement, concrete, supporting plates, and steel channels. ABAQUS software was used to create and evaluate the FE model for the test specimen. It requires for the application of linear and non-linear materials. The two minimal linear material characteristics needed for linear analysis are Young's modulus (E) and Poisson's ratio (ν). For nonlinear analysis, the uniaxial behavior of the steel and concrete is predicted at stresses outside of its elastic range. The input data for steel and concrete in the ABAQUS program is based on results of tests from experimental work.

3.1.1 Concrete Modeling

In order to monitor the nonlinear behavior of RC, the ABAQUS concrete damage plasticity model (CDP) is utilized. The basis of this concept is the plastic flow hypothesis [12]. The CDP model's simulation of the inelastic behavior of concrete is derived from the assumption that isotropically damaged concrete is combined with plasticity characteristics in terms of both compressive and tensile strength. Compressive crushing and tensile cracking are the two main methods of failure control that this model postulates [19].

3.1.2 Uniaxial Compression Properties

Numerous researchers' formulae basically characterized how concrete behaved under uniaxial compression stress. The majority of these equations, though, including those provided by [8] do not describe the entire concrete stress-strain curve. In view of this, the stress-strain equation put forward by [6] is employed to describe the general conduct of the concrete under uniaxial compressive stresses, demonstrated in Eq. (1).

the relationship between σ_c and ϵ_c seen in Fig. (2) (compressive stress and shortening strain indicated as absolute values) is given by the expression:

$$\sigma_c = f_{cm} \frac{ky - y^2}{1 + (k-2)y} \dots\dots (1)$$

In which:
 $k = 1.05 \frac{E_{cm} |\epsilon_{c1}|}{f_{cm}}$; $E_{cm} = 22000 \times (0.1 \times f_{cm})^{0.3}$; $\epsilon_{c1} = 0.0014 \times (2 - e^{(0.024 \times f_{cm})}) - e^{(-0.014 \times f_{cm})}$

$\eta = \frac{\epsilon_c}{\epsilon_{c1}}$; $\epsilon_{cu} = 0.004 - 0.0011 \times [1 - e^{(-0.0125 \times f_{cm})}]$;

σ_c : compressive stress in concrete; k: coefficient factor; ϵ_c : compressive strain in concrete.
 ϵ_{c1} : compressive strain in concrete at the peak stress and ϵ_{cu} : ultimate compressive strain in concrete.

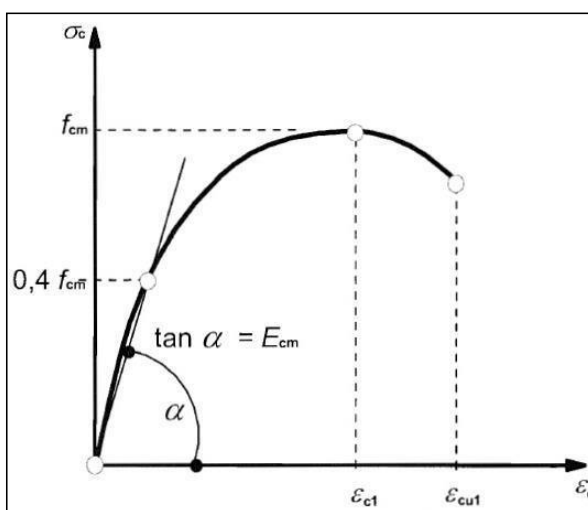


Fig. 2. Compression Concrete Modeling [6].

3.1.3 Uniaxial Tension Behavior

The CDP model were modified to incorporate the tension behavior of concrete illustrated in Fig. (3) utilizing the correlation proposed by [15], and it is described as follows: The stress strain curve, Ascending branch ($\epsilon_1 \leq \epsilon_{cr}$)

$\sigma_1 = E_c \cdot \epsilon_1$ in which:

σ_1 : concrete tensile stress, MPa.

E_c : modulus of elasticity of concrete. ϵ_1 : concrete tensile strain, mm/mm.

ϵ_{cr} : cracking strain of concrete, taken as 0.00008 mm/mm. Descending branch ($\epsilon_1 > \epsilon_{cr}$)

$\sigma_1 = f_{cr} (\epsilon_{cr} / \epsilon_1)^{0.4}$

f_{cr} : cracking stress of concrete, taken as $0.62 \sqrt{f'c}$ (MPa).

$f'c$: were took compressive strength on the data of tested columns.

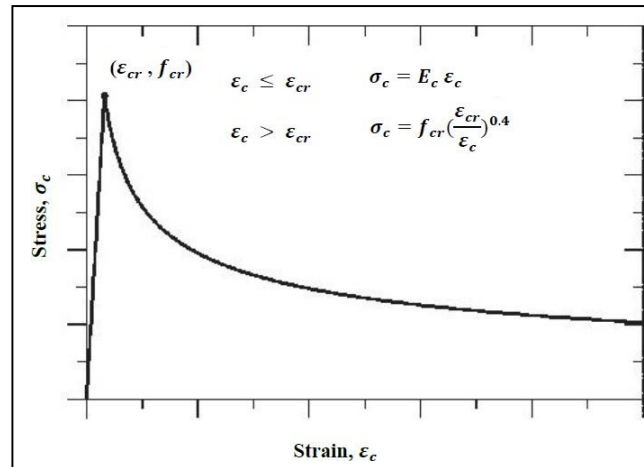


Fig. 3. model for concrete in tension [15].

3.2 Steel Reinforcement and Steel Channel Modeling

In this research, reinforcement and stirrups are made of elastic-perfect plastic. The point at which the material exhibits a linear elastic response up until the yield stress is met is where it begins to plasticize perfectly, as shown in Fig (4).

A nonlinear stress-strain curve can be used with the material behavior that the ABAQUS program offers. The Poisson's ratio and the reinforced modulus of elasticity, which are chosen to be 200×10^3 MPa and 0.3, respectively, characterize the linear isotropic portion. Yield stress serves to determine the bilinear isotropic portion. The examination of steel material includes large inelastic stresses and results in real stress and true plastic logarithmic strain curves. Tables (2) and (3) displays the mechanical characteristics of the steel reinforcement, which consists of longitudinal and transverse reinforcement. and steel channel section mechanical propriety.

For the steel channel modeling, the shell elements used for axisymmetric geometries, 3D shell geometries, and stress/displacement analysis can also be utilized to describe the steel channel in ABAQUS. Full or limited numerical integration can be used with conventional shell elements. The scattered loadings and the mass matrix are perfectly integrated. When the elements are neither twisted nor loaded in an in-plane bending, the reduced integration typically yields accurate results. Running times can be improved by reducing integration, particularly for 3D problem [11] and [3].

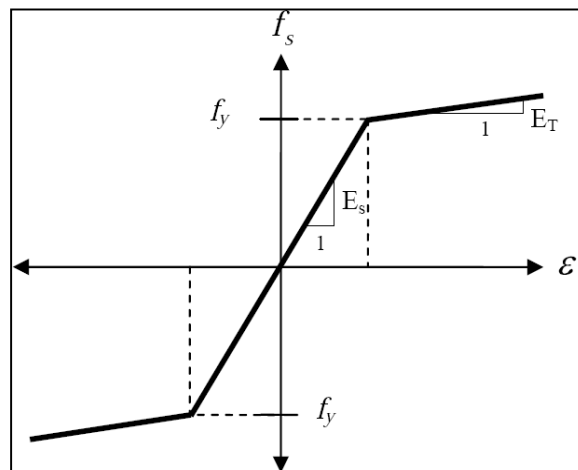


Fig. 4. Model of elastic perfectly plastic steel reinforcing bars [1].

Table 2. Mechanical properties of Steel components.

Nominal Diameter (mm)	Measured Diameter (mm)	Yield Stress* (MPa)	Ultimate Stress* (MPa)	Modulus of Elasticity (MPa)
6	5.81	485	538	200×10 ³
10	9.82	520	620	

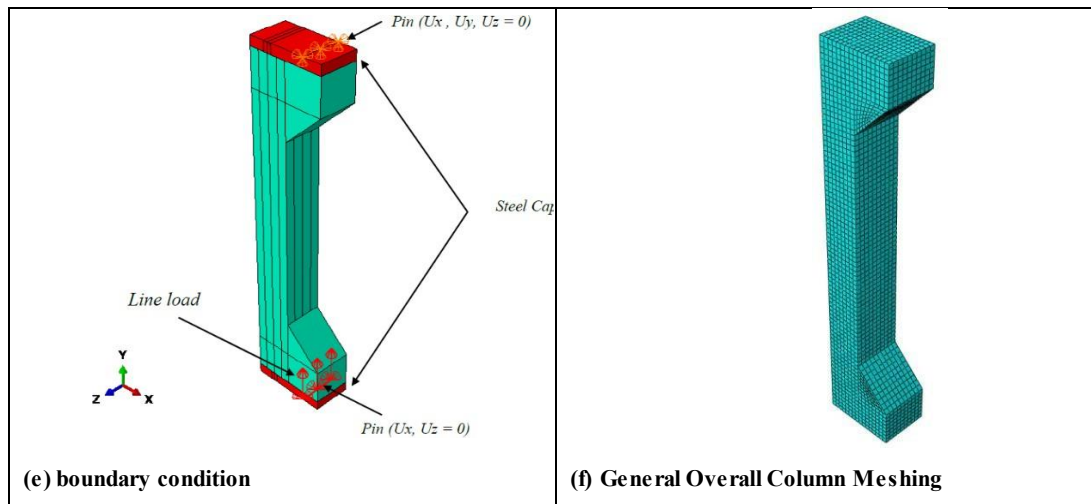
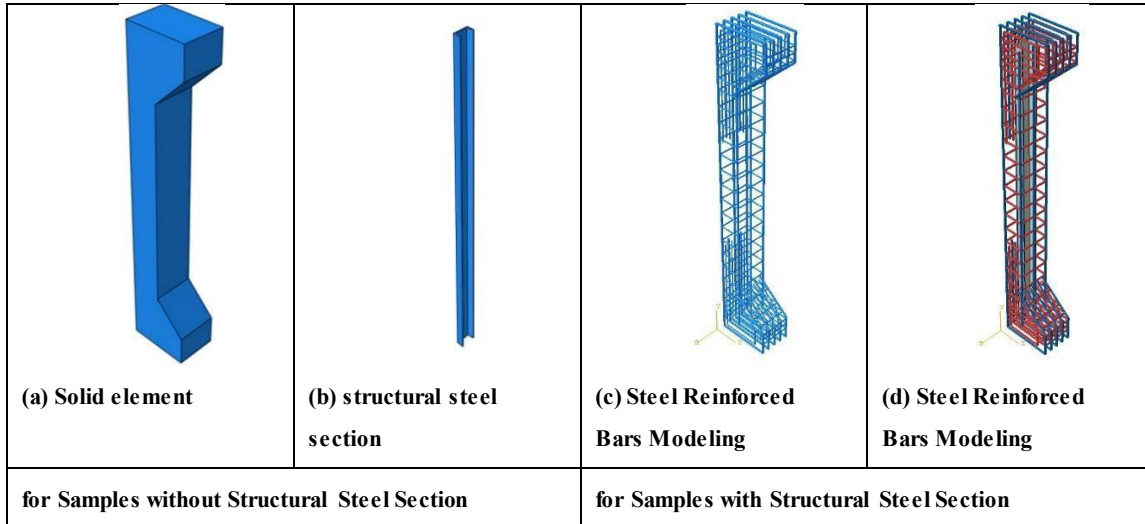


Fig. 5. Modeling of Different Parts of Specimens by ABAQUS Software.

4 Results and Discussion

For the tested columns, the finite element predicts the behavior as shown in Table (4) in terms of ultimate loads and Mid-Span deflection at ultimate capacity.

The load - deflection curves from the experiment and the FE findings are compared in Figs. (6 to 8). RC columns with eccentricity ratios of 0.3 and 0.6 can be identified from the Figures below, which display the experimental and FE

load-lateral mid-height deflection curves. When these curves are interpreted, the initial, post-cracking, and the last parts of the cracking process exhibit good agreement with the findings of the experiments. Over the whole loading range, a generally satisfactory agreement between FE and experimental data was achieved. When the FE curves are compared with the matching experimental curves, it is evident from the figures that during the pre-cracking stages, each column of specimens displayed nearly perfect agreement at ultimate loads.

In general, the load and mid-span deflections curves from the finite element exhibited stiffer behavior when compared to the experimental curves, with a little reduction in the ultimate deflection, as seen in Table (3). The utilization of constitutive models may provide justification for the observed stiffer behaviour of concrete in comparison to control specimens in terms of strain hardening and softening of the tensile strength and lack of microcracks (shrinkages and handling cracks). Additionally, the ABAQUS analysis assumes the assumption that the concrete and reinforcement are entirely bonded, however experimental work would not support this contention.

Due to the obvious effect of the steel section under eccentric load, which results in a compression failure mode, and the fact that the majority of the steel channels are located within the compression zone of the columns cross-section, the presence of steel channels for the second group (Group B) has significantly increased the maximum loads.

Table 3. a summary of the finite element data results for tested columns.

Group	Column Designation	Ultimate load(kN)		FE/EXP Ultimate load ratio	Deflection at midspan (mm)		FE/EXP Deflection ratio
		EXP	FE		EXP	FE	
A	C0E45L1.0	288.35	286.86	0.99	7.65	7.46	0.98
	C0E45L1.2	285.61	285.58	1.00	9.90	9.90	1.00
	C0E45L1.4	245.96	246.35	1.00	8.06	8.59	1.07
	C0E90L1.0	144.36	143.00	0.99	15.25	15.75	1.03
	C0E90L1.2	123.27	121.00	0.98	11.48	10.82	0.94
	C0E90L1.4	101.45	101.39	1.00	13.95	14.24	1.02
B	C1E45L1.0	392.59	392.35	1.00	9.64	10.00	1.04
	C1E45L1.2	288.35	291.00	1.01	7.65	7.65	1.00
	C1E45L1.4	281.96	281.96	1.00	16.44	16.85	1.02
	C1E90L1.0	203.04	203.04	1.00	10.05	10.35	1.03
	C1E90L1.2	169.20	171.11	1.01	10.17	10.30	1.01
	C1E90L1.4	155.17	157.00	1.01	12.14	12.34	1.02

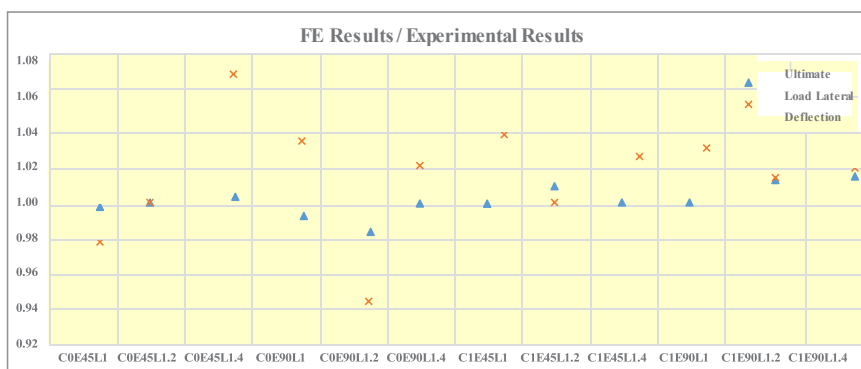
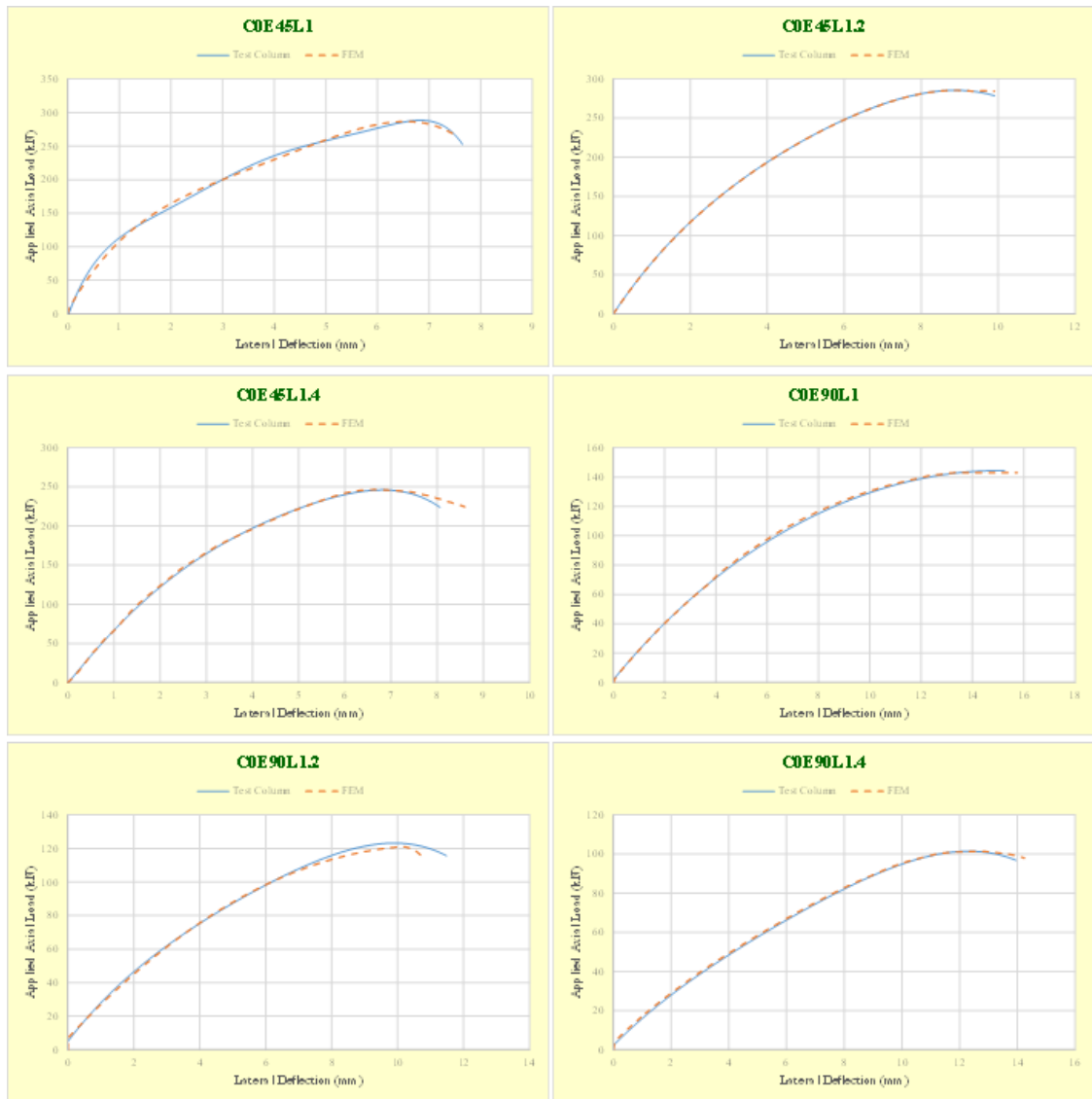


Fig. 6. Comparison ratios for Finite element analysis to the results of experiments for ultimate load capacity and the maximum lateral Deflection.



Figs. 7. Experimental and FE load versus lateral deflection curves for RC columns with e/h 0.3 and 0.6 eccentricity ratios. (Without steel section)

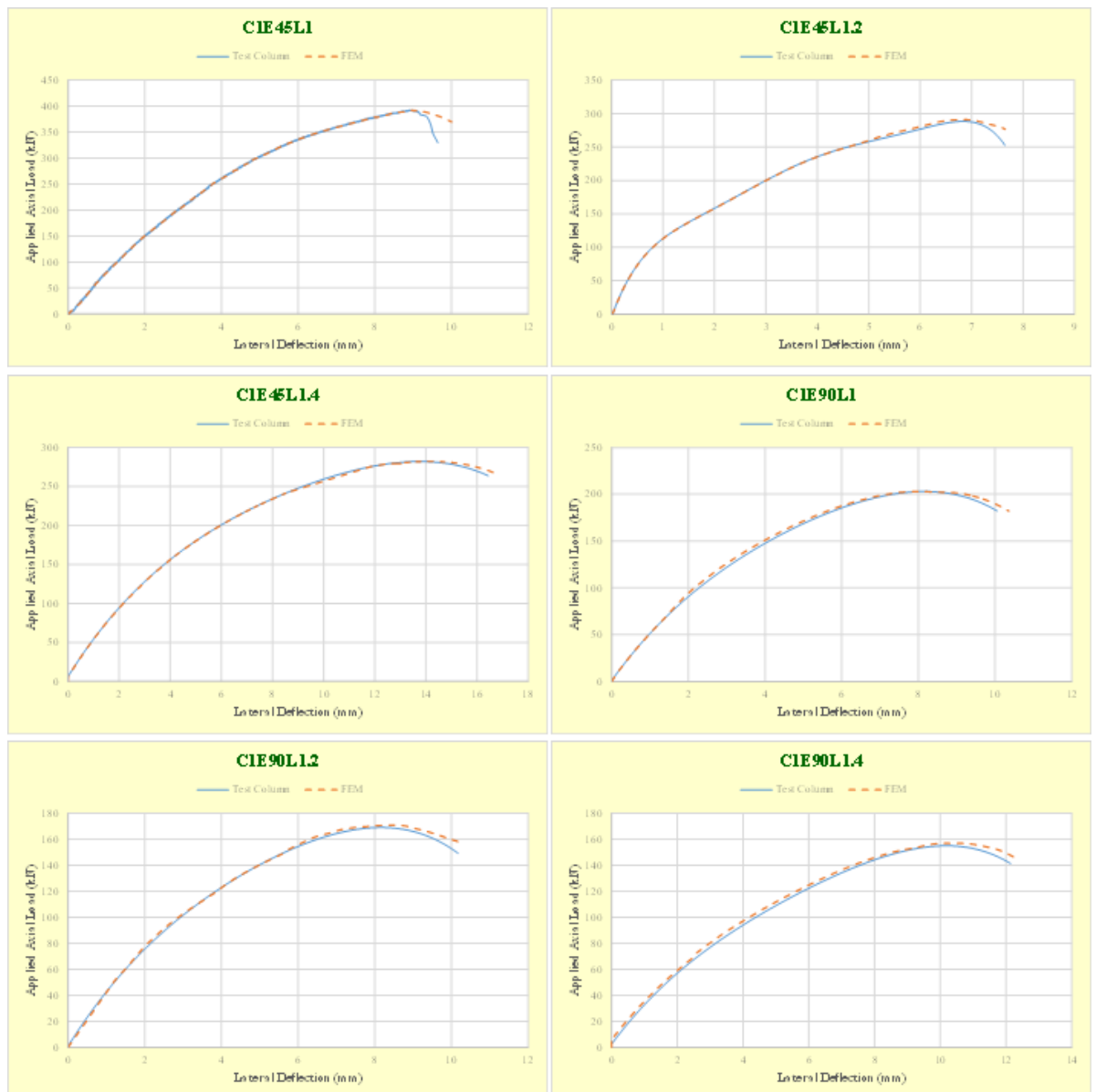


Fig. 8. Experimental and FE load versus lateral deflection curves for RC columns with e/h 0.3 and 0.6 eccentricity ratios. (Without steel section)

5 Stress Distribution

Since it is difficult to map the stress distribution through the components of the slender columns under investigation in the lab, FEA is employed in this situation. The areas of high stress for each tested column were utilized using the von-Mises stress distribution, as shown in Figs. (9).

A colored bar is displayed alongside the models to indicate the gradation. In most cases, the mid-height of columns is where the maximum compressive stress is found.

Additionally, Fig. (10) displays the stresses in the steel embedded channel for the columns under eccentric load. A colored bar at the base of the figures indicates the amount of stress. At the mid-column height, the extreme fiber of the steel channel experiences maximum stress. Moreover, a distinct compression zone for the columns in this group can be noticed in these visuals because of the columns that under compression stresses.

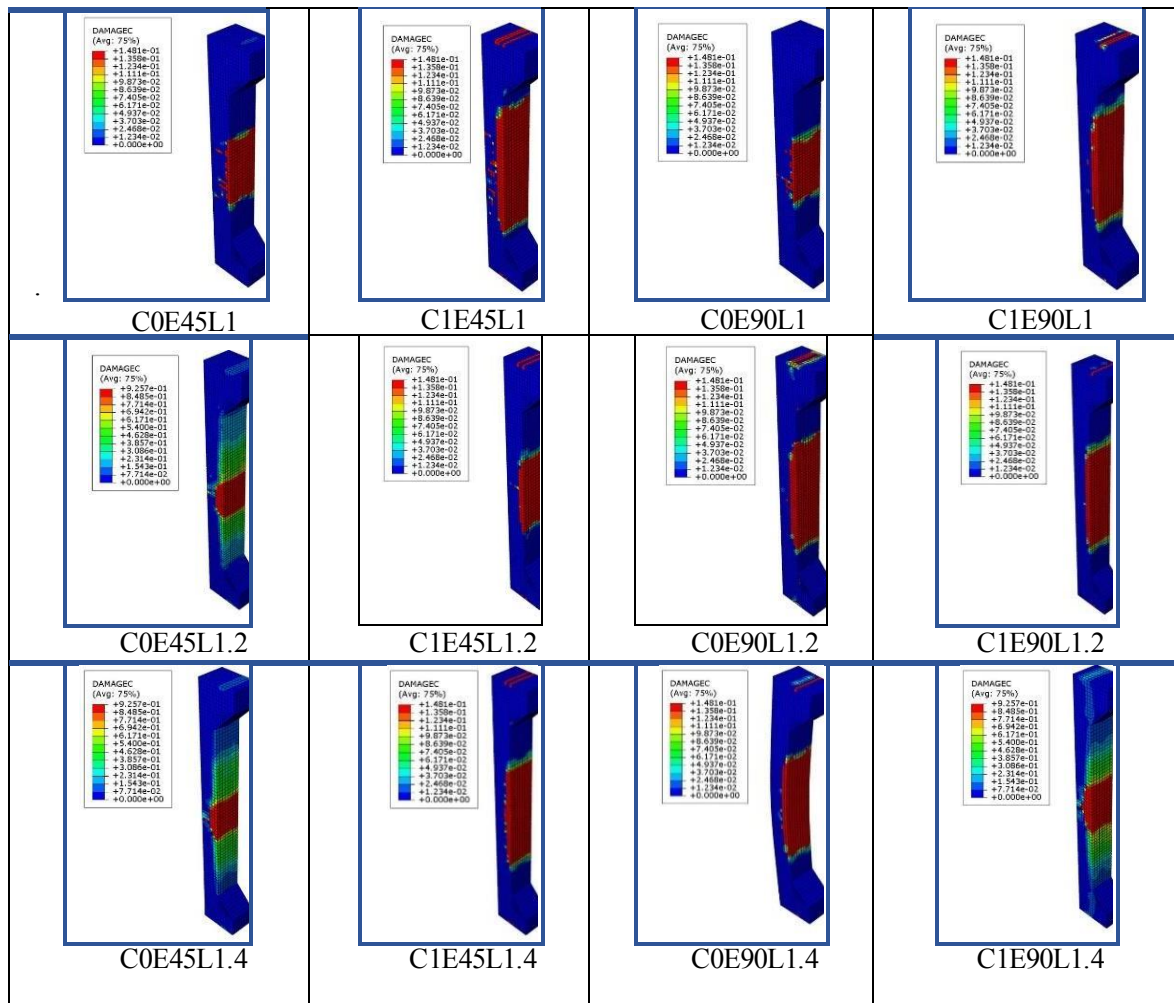


Fig. 9. Stress distribution of columns specimens at ultimate load level.

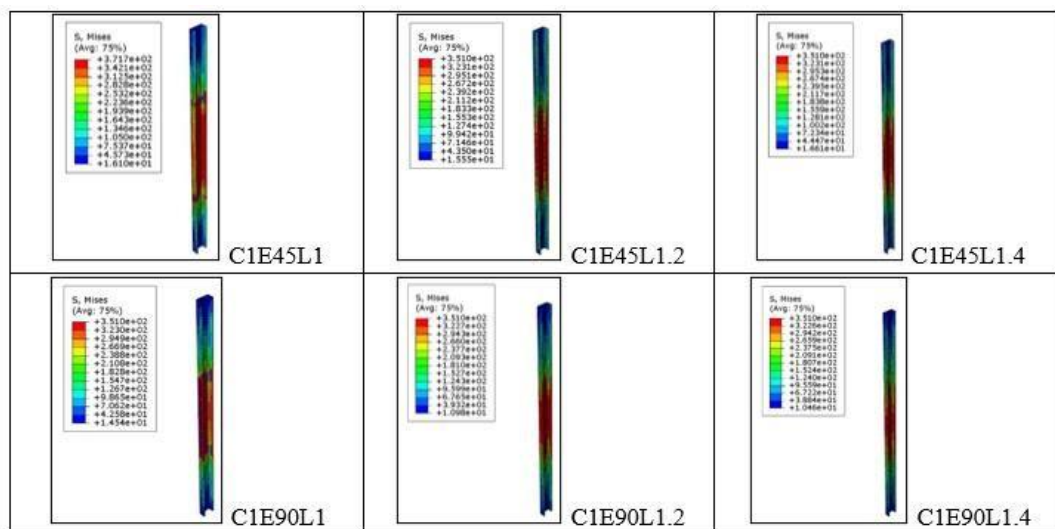


Fig. 10. Steel channel stress distribution for composite columns.

6 Conclusion

The influence of eccentricity, slenderness ratios and concrete strengths on the slender reinforced concrete columns capacities has been studied in this paper. The load-carrying capacity is reduced with an increase of the slenderness ratio.

It has been found that for the eccentrically loaded columns, load-carrying capacity decreases dramatically as eccentricity increases but is not greatly impacted by concrete strength. An analytical method to compute the ultimate strength of slender reinforced concrete composite columns has been proposed.

Reinforced Concrete Columns without Embedded Steel Channels:

1. Slenderness Ratio Effect:
 - a. As the slenderness ratio (effective length divided by the least lateral dimension) increases, the axial load-carrying capacity of slender columns decreases.
 - b. Slender columns are more susceptible to buckling, and their load-carrying capacity is significantly affected by second-order phenomena, such as P-delta effects and member imperfections.
2. Eccentricity Effect: Columns subjected to eccentric loading (applied load not acting through the centroid) experience additional bending moments, leading to reduced axial capacity.

Reinforced Concrete Columns with Embedded Steel Channels:

1. Slenderness Ratio Effect:
 - a. Embedding steel channels within the concrete column can enhance its slenderness ratio by providing additional lateral support.
 - b. The embedded steel channels can increase the critical buckling load and improve the overall stability of the slender column.
2. Eccentricity Effect: The presence of embedded steel channels can mitigate the adverse effects of eccentric loading by providing additional stiffness and resistance to bending.
3. Combined Effect:
 - a. The combined use of reinforced concrete and embedded steel channels can result in a stronger and more stable column system.
 - b. The interaction between concrete and steel can lead to a composite behavior that enhances the load-carrying capacity and ductility of the column.
 - c. It's important to note that the actual behavior and capacity of columns depend on various factors, including material properties, construction details, and specific design considerations. Professional structural engineers typically use advanced analysis and design methods to optimize column performance based on project requirements and safety standards. Additionally, local building codes and standards play a crucial role in determining the design parameters for reinforced concrete columns.

References

1. ABAQUS Version 2019. [Computer software]. Assault Systems. Waltham. MA.
2. ABAQUS: ABAQUS Analysis User's Manual Version 2019. Assault Systems.
3. Ellobode, E. (2014). Finite Element Analysis and Design of Steel-Concrete Composite Bridges.
4. Tanta University, Egypt: Elsevier Inc.
5. Ellobody, E., Young, B., & Lam, D. (2011). Eccentrically loaded concrete encased steel composite columns. *Thin-Walled Structures*, 49(1), 53–65. <https://doi.org/10.1016/j.tws.2010.08.006>
6. Eurocode2. (1992). Eurocode 2: Design of concrete structures-Part 1. General rules and rules for buildings. *British Standards*, 194.
7. Lai, B., Liew, J. Y. R., & Xiong, M. (2019). Experimental study on high strength concrete encased steel composite short columns. *Construction and Building Materials*, 228, 116640.
8. Mander, J. B., Priestley, M. J. N., & Park, R. (1988). Theoretical stress-strain model for confined concrete. *Journal of Structural Engineering*, 114(8), 1804–1826.
9. Mohammed, G. K., Sarsam, K. F., & Korkess, I. N. (2020). Modeling the Flexural Performance of Reinforced Concrete Built-up Beams. *IOP Conference Series: Materials Science and Engineering*, 745(1), 12108.
10. Oukaili, N. K., & Abdullah, S. S. (2017). Behavior of Composite Concrete-Castellated Steel Beams under Combined Flexure and Torsion. *APFIS2017-6th Asia-Pacific Conference on FRP in Structures*, 19–21.
11. Tysmans, T., Wozniak, M., Remy, O., & Vantomme, J. (2015). Finite element modelling of the biaxial behaviour of high-performance fibre-reinforced cement composites (HPFRCC) using Concrete Damaged Plasticity. *Finite Elements in Analysis and Design*, 100, 47–53.
12. Wang, Q., Shi, Q., & Tao, Y. (2016). Experimental and numerical studies on the seismic behavior of steel reinforced concrete compression-bending members with new-type section steel. *Advances in Structural Engineering*, 19(2), 255–269.
13. Wang, Q., Shi, Q., & Tian, H. (2015). Seismic behavior of steel reinforced concrete (SRC) joints with new-type section steel under cyclic loading. *Steel and Composite Structures*, 19(6), 1561–1580.
14. Wang, T., & Hsu, T. T. C. (2001). Nonlinear finite element analysis of concrete structures using new constitutive models. *Computers & Structures*, 79(32), 2781–2791.
15. Weng, C. C., & Yen, S. I. (2002). Comparisons of concrete-encased composite column strength provisions of ACI code and AISC specification. *Engineering Structures*, 24(1), 59–72. [https://doi.org/10.1016/S0141-0296\(01\)00067-0](https://doi.org/10.1016/S0141-0296(01)00067-0)